IEEE Access
Multidisciplinary | Rapid Review | Open Access Journal

Received August 29, 2021, accepted October 9, 2021, date of publication November 2, 2021, date of current version November 10, 2021.

Digital Object Identifier 10.1109/ACCESS.2021.3124786

Rule-Based Control of Battery External Heating for Electric Vehicle During Driving at Low Temperatures

SHUPENG ZHANG[1], (Member, IEEE), AND WENJING SHEN[2], (Member, IEEE)
[1]College of Urban Transportation and Logistics, Shenzhen Technology University, Shenzhen 518118, China
[2]Sino-German College of Intelligent Manufacturing, Shenzhen Technology University, Shenzhen 518118, China

Corresponding author: Wenjing Shen (shenwenjing@sztu.edu.cn)

This work was supported by the Natural Science Foundation of Top Talent of the Shenzhen Technology University (SZTU) under Grant 2018010801007.

ABSTRACT As the only power source of pure electric vehicles, lithium-ion batteries play an important role in vehicle powertrain systems. However, lithium-ion batteries have a significant reduction in capacity and power capability at low temperatures, which results in a greatly shortened driving range and poor acceleration of the vehicle. In this study, a rule-based battery external heating control strategy was developed to heat the battery during driving. An electrothermal film was affixed to the surface of each cell as an external heating material that was powered by the battery. An equivalent circuit model combined with a thermal model was established to simulate the electrical and thermal dynamics of the system with sufficiently high accuracy, and control rules were developed based on the model. The optimal solution was obtained by adopting the dynamic programming algorithm to optimize the trade-off between temperature rise and energy consumption and maximize the total driving range under different low temperature driving conditions. Simulation results on the experimentally validated model show that the vehicle with the proposed control algorithm increased the total driving range by 18.6% to 220% for different driving conditions at cold to extremely cold temperatures compared with the vehicle without external heating. Furthermore, the rule-based control showed a 1.1% to 4.4% improvement compared with the maximum (constant) power heating method.

INDEX TERMS Lithium-ion battery, external heating, electric vehicle, driving range, rule-based control, dynamic programming.

I. INTRODUCTION

As environmental issues and the energy crisis have continued to intensify, electric vehicles (EVs) have become a promising alternative to greatly reduce emissions and fossil fuel consumption. With their continuously improving energy efficiency, safety and driving range, and promotion by government policies, the market share of EVs has increased significantly during the last decades [1]. Under the requirements of vehicle performance, lithium-ion batteries have become increasingly widely used as traction batteries in EVs due to their advantages of high energy density, low self-discharge, and long cycle life [2], [3]. However, there is a nonnegligible drawback of lithium-ion batteries in that their performance is greatly reduced at low temperatures. This is mainly due to poor electrolyte conductivity, poor lithium intercalation kinetics at the electrode surfaces, and poor ionic diffusion in the electrode bulk [4]. The resulting poor performance is reflected by the dramatically increased electrochemical impedance [5], reduced capacity and derated charging and discharging power limits at low temperatures. Because the traction battery is the only power source of pure EVs, the reduced performance has a significant impact on vehicle behavior, leading to a shortened driving range, poor acceleration and loss of regenerative braking energy. A range loss of approximately 40% to 60% at −20°C was reported compared with normal temperature conditions [6], [7]. Therefore, a battery heating system and strategy for cold weather conditions are urgently needed to guarantee satisfactory vehicle performance.

The two commonly used approaches for battery heating are external and internal heating [8], [9]. External heating refers

The associate editor coordinating the review of this manuscript and approving it for publication was Christopher H. T. Lee.

to heating the battery by external heating sources through heat transfer, and the commonly used external heating methods include air heating, liquid heating and electrothermal element heating [10]. For air heating, a battery pack is usually equipped with a resistive heater powered by either an onboard DC/DC converter or an external power source to generate heat, and a fan to create a convective flow around the pack [11], [12]. The main problem with air heating is that the low thermal conductivity leads to a relatively long heating time. Furthermore, convective heating may also cause a large temperature gradient between different cells, which can be harmful for pack operation. For liquid heating, the heating system mainly consists of a heater, heat exchanger, pump and circulation pipes. Heat is transferred from the liquid to the battery through the heat exchanger. Because liquid has a higher thermal conductivity than air, the heating rate could be greatly increased; however, the sealing issue makes the design of its system structure more challenging. There are several different approaches to electrothermal element heating. Zhang *et al.* [13] used a positive temperature coefficient (PTC) material to form external heating plates. The PTC plates were mounted under the battery modules and powered by an external power supply. In addition, electric fans were installed to facilitate air circulation, thereby improving the preheating effect. However, the major drawbacks of PTC plate heating are the non-uniform temperature distribution between the cells and the relatively slow heating rate. Lei *et al.* [14] presented a wide-line metal film method for battery heating in which the films were placed on the surface of the cells. Compared with an electrothermal plate, the electrothermal film has the advantage of a much smaller thickness which makes it possible to attach it between the cells and guarantees a more uniform temperature distribution. Alaoui and Salameh [15] employed a Peltier effect element as an electrothermal material that can transfer heat from the heat sink to the battery cells. The advantage of Peltier element heating is that the temperature rise rate can be controlled by the amplitude of the electrical current passing through the Peltier element, which enables accurate control of the battery temperature. Chen and Li [16] constructed a heating module using a pulsating heat pipe with TiO_2 nanofluid as the working medium. It was confirmed that rapid preheating and temperature uniformity can be achieved due to the highly efficient bidirectional thermal transfer and thermal conductivity characteristics of the pulsating heat pipe.

In contrast to external heating, the basic idea of internal heating is to utilize the internal resistance of the battery to generate heat by imposing a current through the battery. There are two types of current sources, alternating current and direct current. The sinusoidal alternating current heating method has been widely investigated. It has a relatively fast heating rate and less impact on battery life [8]. Ruan *et al.* [17] developed a rapid AC heating strategy with an optimal frequency based on a constant polarization voltage. An average temperature rise rate of 3.73°C/min with an essentially uniform temperature distribution was reported. Zhang *et al.* [18] investigated the battery impedance spectrum at different temperatures and developed a multi-stage AC heating strategy in which the frequency of the alternating current remains constant, but the magnitude changes based on the temperature. The proposed method can maximize the heat generation at different temperatures, thus minimizing the heating time without incurring the Li-plating phenomenon. However, AC heating also has the limitation of requiring outside AC generation facilities, leading to difficulty in onboard implementation. Shang *et al.* [19] designed a high-frequency sine-wave heater based on resonant LC converters on an EV, which enables onboard self-heating of the batteries. Li *et al.* [20] developed a novel driving circuit for EVs and proposed a triple-module separated invert (TMSI) mode to rapidly heat the battery pack. Heating can be performed during parking and EV driving. Shang *et al.* [21] proposed a high-frequency AC heater based on buck-boost conversion and developed a heating strategy based on a thermoelectric model. They verified that increasing the AC-heating frequency can significantly improve the heating speed and efficiency. However, in general, AC heating devices are bulky and expensive.

The other internal heating method is DC heating, which uses the battery discharge current to generate heat. However, due to the polarization phenomenon, a long discharge current with a large rate can result in a significant voltage drop in the battery and further reduce the battery's life [22]. Du *et al.* [23] developed an optimal control method using the weighted capacity fade rate and heating time as the cost function. However, this strategy took a constant discharge current limit as the hard constraint, which led to conservative results, and the battery temperature rise rate was relatively slower than AC heating. Ruan *et al.* [24] considered the discharge cut-off voltage as one of the constraints, formulated the heating time and capacity degradation as dual objectives, and used a multi-objective genetic algorithm to solve the optimal control problem. It achieved a significantly improved average temperature rise rate with no substantial lifetime reduction. To reduce the impact on battery life, Qin *et al.* [25] modified the one-direction current to a bidirectional pulsed current, and found that bidirectional pulse heating can fully utilize the internal resistance of the battery and may reduce the impact on battery life through fast reverse depolarization. Furthermore, Wang *et al.* [26] invented an "All climate battery" (ACB) by embedding a nickel foil inside the cell as a heating resistance and achieved a fast temperature rise rate of approximately 1°C/s, consuming only 3.8% of the cell capacity. This approach significantly shortens the heating time, but it has to modify the internal structure of the cell, which results in higher cost and system complexity.

In summary, recent studies on battery heating at cold temperatures have mainly focused on improving the heating efficiency during preheating but they lack a heating strategy for driving conditions. Although continuous progress has been made in terms of higher heating rate, less battery capacity

fade, and lower cost, there is always a trade-off between shortening heating time and preventing battery life reduction. In order to protect the battery from being overcharged or overdischarged, and to avoid significant battery life reduction, the heating power could not be large regardless of the heating strategy, and the resulting long preheating process brings extreme inconvenience to the driver. Furthermore, the required heating devices are usually not suitable for onboard implementation.

In this study, a rule-based battery heating strategy to optimize the heating process during driving is developed. An external heating method with an electrothermal film is adopted, and the battery provides the required power. Instead of shortening the preheating time before driving, this strategy employs an onboard heating control during driving to recover the battery capacity and increase the driving range. With the rule-based control strategy, the heating power depends on the battery and environmental conditions, and the vehicle's traveling distance can be maximized before the battery is out of available energy. In addition, the duration of the external heating during driving can be much longer than during preheating; therefore, the required amount of heating power is significantly less than during preheating, which brings significant benefits to battery health.

The remainder of this paper is organized as follows. Section II introduces the battery heating system configuration and presents a mathematical model, which includes an equivalent circuit model of the battery and a thermal model for the battery and heater. Section III proposes a rule-based control strategy and solves the optimal problem under a special driving condition. The associated experimental validation and simulation results are presented in Section IV, and several conclusions are drawn in Section V.

II. SYSTEM MODELING

A. SYSTEM CONFIGURATION

A lithium ferrous phosphate (LFP) pouch cell is taken as the object in this study. The battery pack equipped on the target vehicle consists of three parallels, and each parallel has 100 cells in series connection. Under this particular configuration, the target vehicle achieves approximately 125 miles with a fully charged battery in normal temperatures. The cell parameters are shown in Table 1.

An electrothermal film with a polymide as the base material was chosen as the external battery heater. The film was affixed to the surface of each pouch, as shown in Figure 1 (a). The films are connected in parallel in each battery module, as shown in Figure 1 (b), and consume the energy from the cells through a DC/DC converter which is controlled in power mode by the Battery Management System (BMS). In this study, we replaced BMS with a Speedgoat rapid control prototype (RCP) for the purpose of control algorithm development. The parameters of the electrothermal film are listed in Table 2.

TABLE 1. Cell parameters.

Parameter	Value
Mass (kg)	1.2
Length (mm)	227
Width (mm)	161
Thickness (mm)	15
Nominal voltage (V)	3.29
Charge cut-off voltage (V)	3.65
Discharge cut-off voltage (V)	2.00
Capacity (Ah)	60
Energy capacity (Wh)	193.63
Operating range (℃)	-30-55
Specific heat capacity (J/Kg·K)	1130

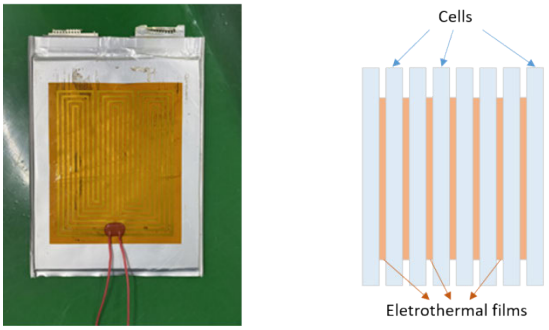

FIGURE 1. (a) Front view, a battery cell with electrothermal film affixed to the surface; (b) Side view, a battery module equipped with the cells and external heater.

TABLE 2. Electrothermal film parameters.

Parameter	Value
Mass (g)	37.5
Length (mm)	150
Width (mm)	120
Thickness (mm)	0.15
Rated voltage (V)	12
Rated power (W)	20
Specific heat capacity (J/Kg·K)	1220
Operating range (℃)	-190-205

B. EQUIVALENT CIRCUIT MODEL

The battery cell is modeled using the equivalent circuit method, as shown in Figure 2.

The equivalent circuit model uses the first-order RC circuit approach, which has satisfied accuracy and requires a relatively low computational load for control design. In the circuit, R_o is the ohmic resistance; R_p is the polarization resistance, and C_p is the polarization capacitance. U_{OCV} denotes the open-circuit voltage of the cell and U denotes the output voltage of the cell. U_o is the voltage drop on R_o; U_p is the polarization voltage on R_p, and I is the discharge current. The dynamics of the equivalent circuit model can be

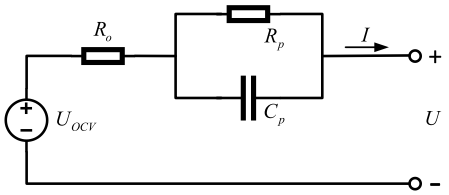

FIGURE 2. Equivalent circuit model of the battery cell.

represented by (1).

$$\begin{cases} C_p \dfrac{dU_p}{dt} + \dfrac{U_p}{R_p} = I \\ U_{OCV} - IR_o - U_P = U \end{cases} \tag{1}$$

All these parameters could be temperature and State of Charge (SOC) dependent. A set of modified hybrid pulse power characteristic (HPPC) tests was performed to identify the values of these parameters. First, a standard HPPC test set both the charge and discharge pulses at 5C for 10s. Since at low temperatures, the charge and discharge capability of the cell is significantly degraded, the pulse was modified to 1C for 50s. Second, normally, the testing points are chosen every 10% of SOC; however, the State of Energy (SOE) will be used instead of SOC in this study for the purpose of control design. Hence, the testing points were chosen every 10% of the SOE. Third, the modified HPPC tests were performed from −30°C to +30°C every 5°C to cover most of the operational temperature range of the battery. Finally, each test was performed on 10 cells and repeated three times. An average value was taken as the final result to reduce the case-by-case variation and part-by-part variation.

The testing data were analyzed using MATLAB parameter estimation toolbox with the least squares approach. The results showed that the variation of ohmic resistance at different SOEs was negligible; thus, R_o was treated as temperature dependent only. Figure 3 shows the ohmic resistance as a function of temperature. It can be seen that R_o increases as the temperature decreases, and increases dramatically when the temperature decreases below 0°C.

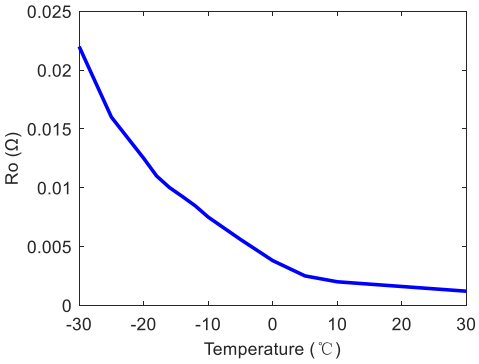

FIGURE 3. Ohmic resistance at different temperatures.

Figure 4 shows the polarization resistance as a function of the temperature and SOE. R_p has a similar property

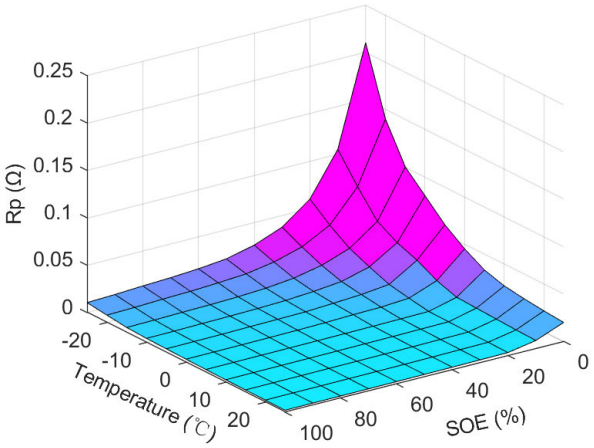

FIGURE 4. Polarization resistance at different temperatures and SOE.

to R_o with respect to temperature; that is, when the temperature decreases, the resistance increases. This is one of the essential reasons for the relatively low capacity of the cell at low temperatures. However, unlike the ohmic resistance, the polarization resistance exhibits a strong relationship with the SOE. As the SOE decreases, R_p increases gradually, and it significantly increases when the SOE approaches 0%.

The cell energy capacity is defined as the total available energy at a certain temperature. Note that in addition to the temperature, the capacity also depends on the discharging rate. At higher discharge rates, due to the polarization phenomenon, the output voltage of the cell drops to a lower level and will reach the cut-off voltage earlier. Here, the capacity tests were performed at 0.3C rate to be consistent with our control design case. Figure 5 shows the energy capacity of the cell at different temperatures. It can be observed that at 23°C the cell has the highest energy capacity. Below 0°C the capacity shows a significant degradation, and at −30°C the capacity decreases by more than 50%.

During discharging, the consumed energy E_c is the integral of the instantaneous total consumed power over time. The instantaneous consumed power can be classified by three types, as shown on the right side of (2). The first type is the load power, which is the power consumed by the propulsion system of the vehicle and accessory loads, denoted by P_{load}. The second type is the Joule heat generated by the internal resistance of the cell, which includes the ohmic resistance heat generation I^2R_o and polarization resistance heat generation $I_p^2R_p$. The third type is the heating power consumed by the external heating system, denoted by P_{heat}.

$$E_c = \int Pdt = \int \left(P_{load} + I^2R_o + I_p^2R_p + P_{heat}\right)dt \tag{2}$$

Once the total consumed energy is determined, the instantaneous SOE can be obtained using the following equation:

$$SOE = SOE_0 - \frac{E_c}{E_t} \tag{3}$$

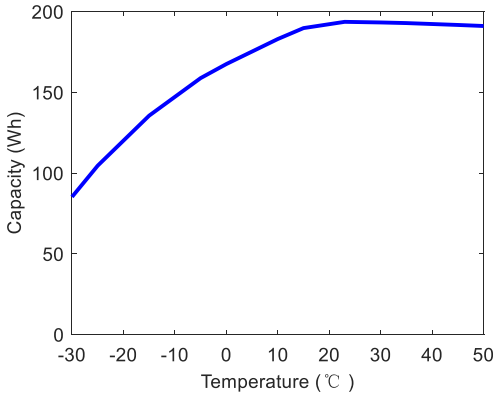

FIGURE 5. Cell energy capacity.

where SOE_0 is the initial state of energy, and E_t is the total available energy capacity of the battery cell which can be determined from Figure 6 if the instantaneous cell temperature is available.

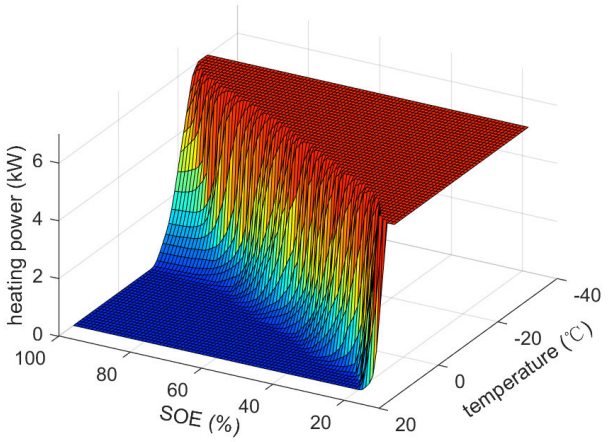

FIGURE 6. Optimal heating power at −20°C.

C. THERMAL MODEL

The thermal model includes an internal heat generation model and the external heating model. The simplified internal heat generation model is given by the following equation:

$$Q = Q_j + Q_e = I\left(U_{OCV} - U\right) + IT\frac{\partial U_{OCV}}{\partial T} \tag{4}$$

where Q is the total heat generated internally during charging and discharging. Q_j is the Joule heat generated by the current flowing through the resistance, which is discussed in subsection B. Q_e is the reversible entropic heat generated due to entropy potential. The external heat generation model shows the heat transfer between the cell and the electrothermal film through thermal convection, and the transferred power Q_{tr} can be expressed by (7):

$$Q_{tr} = h_1A_1\left(T_h - T\right) - h_2A_2\left(T - T_\infty\right) \tag{5}$$

where h_1 is the heat transfer coefficient of the cell to the electrothermal film and h_2 is the heat transfer coefficient of the cell to the air. A_1 is the surface area of the electrothermal film and A_2 is the area of the cell exposed to air. T is the temperature of the cell; T_h is the temperature of the electrothermal film, and T_∞ is the environmental temperature. Then, the complete thermal model of the system for a single cell and heater can be described by (6) and (7):

$$\begin{aligned} mC\frac{dT}{dt} &= I^2R_o + I_p^2R_p + IT\frac{\partial U_{OCV}}{\partial T} \\ &\quad + h_1A_1\left(T_h - T\right) - h_2A_2\left(T - T_\infty\right) \end{aligned} \tag{6}$$

$$m_hC_h\frac{dT_h}{dt} = \eta P_{heat} - h_1A_1\left(T_h - T\right) \tag{7}$$

where m is the mass of a cell, and m_h is the mass of an electrothermal film. C is the thermal capacity of the cell, and C_h is the thermal capacity of the electrothermal film. η is the heater efficiency. Parameters C, C_h, h_1, and h_2 can be obtained by constant-power heating and constant-temperature cold soak tests, respectively.

D. MODEL DISCRETIZATION AND REDUCTION

Normally, the electric vehicle achieves less range on highway driving than local driving because the driving resistance is larger when the vehicle speed is higher, and the efficiency of the traction motor does not vary significantly. The range issue is more severe with highway driving in cold weather. In this study, a special case of constant speed driving on a highway was studied for the convenience of rule-based control design. The chosen constant speed was the average vehicle speed of the Highway Fuel Economy Driving Schedule (HWFET) driving cycle, which is 48 mph. During constant speed driving, the load power is also constant, and was 17.6 kW for the target vehicle. After a short period of time the dynamic response of the RC circuit has achieved the approximate steady state, which means that the current flowing through the polarization resistor can be assumed to be equal to the current flowing through the ohmic resistor, that is, $I_p = I$. Hence the equivalent circuit model can be reduced from first-order to zero-order. To discretize the model, the current and the output voltage of the cell at the k^{th} step can be obtained by solving the following two equations:

$$I\left(k\right) = \frac{p_{load}\left(k\right) + p_{heat}\left(k\right)}{U\left(k\right)} \tag{8}$$

$$U\left(k\right) = U_{OCV}\left(k\right) - I\left(k\right)\left(R_o\left(k\right) + R_p\left(k\right)\right) \tag{9}$$

Then, equation (2) can be discretized to (10) with sampling time Δt.

$$\begin{aligned} E_c\left(k+1\right) = E_c\left(k\right) + \Big[&P_{load}\left(k\right) + I^2\left(k\right)\left(R_o\left(k\right) + R_p\left(k\right)\right) \\ &+ P_{heat}\left(k\right)\Big]\Delta t \end{aligned} \tag{10}$$

Based on the open-circuit voltage test results, the value of $\partial U_{OCV}/\partial T$ is in the range of 0.05∼0.2 mV/°C. During normal driving, the entropic heat does not contribute too much compared with the other terms in equation (6) and can be ignored for the convenience of calculation. Similarly, because the mass of the electrothermal film is much smaller

than that of the cell, the term containing m_h can be ignored when equations (6) and (7) are summed, which means that the total net heat will contribute to the temperature rise of the cell. Then the discrete-time state equation for the cell temperature can be obtained (11), as shown at the bottom of the page.

Figure 6 shows that the cell's energy capacity is a function of cell temperature. To linearize this function, the cell's energy capacity can be written as:

$$E_t(k) = a(k)\,T(k) + b(k) \tag{12}$$

where coefficients $a(k)$ and $b(k)$ depend on the cell temperature at the k^{th} step.

Finally, by combining equations (3), (10), (11) and (12), the discrete-time state equation for cell SOE can be derived in (13), as shown at the bottom of the page.

Note that the reduced-order discrete time system model is only used for the control design in the following section. For simulation validation, a continuous time model was used.

III. EXTERNAL HEATING CONTROL

During driving, the battery is continuously discharged and charged. Due to internal resistance, the generated Joule heat will increase battery temperature gradually, even without external heating. However, this internal heating rate is often low meaning the battery will run out of the available energy before it reaches the normal temperature. With the external heating algorithm, a small portion of the discharging current of the battery is utilized to generate extra heat with the electrothermal film, which has a much larger resistance than the cell, and the battery temperature rise rate can be greatly increased.

However, there is a trade-off between the temperature rise rate and the consumed heating energy. If the external heating power is small, the battery heating process can be slow, and by the end of driving, a certain amount of "hidden" energy cannot be used because of the low cell temperature. In contrast, if the external heating power is large, the heating process could be fast, meaning the battery will have a complete capacity recovery, but more energy will be "wasted" by the external heating. Furthermore, instantaneous power for propulsion could be limited. Hence there exists an optimal choice of external heating power, and in this study, the control target is chosen to maximize the range of the vehicle. A rule-based control strategy was designed to achieve the control target as illustrated in the following subsections.

A. RULE-BASED CONTROL

As shown in Figure 6, the capacity of the cell has almost reached the nominal value when its temperature is above 15°C, hence, it is not necessary to continue heating the battery after the temperature reaches this point. For rule-based control, S_{heat} is defined in (14) to denote the heating status. When $S_{heat} = 1$, the heater is on and when $S_{heat} = 0$, the heater is off. A hysteresis of 1°C was taken to avoid frequent switching on and off of the heating system.

$$S_{heat}(k) = \begin{cases} 0 & \text{if } T \geq 15^{\circ}\text{C and } S_{heat}(k-1) = 1 \\ & \text{or } T \geq 14^{\circ}\text{C and } S_{heat}(k-1) = 0 \\ 1 & \text{if } T < 15^{\circ}\text{C and } S_{heat}(k-1) = 1 \\ & \text{or } T < 14^{\circ}\text{C and } S_{heat}(k-1) = 0 \end{cases} \tag{14}$$

Then the rules for controlling heating power can be expressed as

$$P_{heat}(k) = \begin{cases} 0 \\ \qquad \text{if } S_{heat} = 0 \\ \max\left(P_{\min}, P_{dis} - P_{load}\right) \\ \qquad \begin{cases} \text{if } S_{heat} = 1 \text{and} \\ P_{load} > P_{dis} - P_{opt} \end{cases} \\ P_{opt} \\ \qquad \begin{cases} \text{if } S_{heat} = 1 \text{ and} \\ P_{ch} - P_{opt} \leq P_{load} \\ \leq P_{dis} - P_{opt} \end{cases} \\ \min\left(P_{\max}, P_{ch} - P_{load}\right) \\ \qquad \begin{cases} \text{if } S_{heat} = 1 \text{ and} \\ P_{load} < P_{ch} - P_{opt} \end{cases} \end{cases} \tag{15}$$

When the heater is on, the heating power is determined by the rules based on the level of demanded load power. These rules can be explained by the following three cases:

Case 1. The load power is larger than the difference between the maximum discharging power of the battery pack and the optimal heating power, where the optimal heating power is explained in Case 2. In this case, the performance of the vehicle has a higher priority than heating the battery; thus, the power for propulsion should be guaranteed first and the remaining available discharging power can be used for

$$T(k+1) = T(k) + \frac{I^2(k)\left(R_o(k) + R_p(k)\right) + \eta P_{heat}(k) - h_2 A_2\left(T(k) - T_\infty\right)}{mC}\Delta t \tag{11}$$

$$SOE(k+1) = SOE(k) + \frac{a(k)\left[I^2(k)\left(R_o(k)+R_p(k)\right)+\eta P_{heat}(k)-h_2A_2\left(T(k)-T_\infty\right)\right]E_c(k) - \left[P_{load}(k)+I^2(k)\left(R_o(k)+R_p(k)\right)+P_{heat}(k)\right]E_t(k)}{mC}\Delta t \tag{13}$$

heating, unless the remaining part is less than the minimum power of the heater.

Case 2. The load power is medium and the optimal heating power can be achieved without affecting the vehicle's performance. In this case, the heating power should follow the optimal power, which can maximize the driving range of the vehicle or minimize the energy loss of the battery. The optimal solution is described in the following section.

Case 3. During regenerative braking, if the difference between the load power (absolute value) and maximum charging power (absolute value) of the battery is larger than the optimal heating power, it does not make sense to throw the remaining part of the regenerative power away. The regenerative power is taken to the greatest extent until it reaches the maximum power of the heater.

B. SUBOPTIMAL CONTROL DESIGN

Our main purpose is to maximize the range of the vehicle when driving in low temperatures. Note that maximizing the vehicle's range is equivalent to maximizing the available energy of the battery, or in other words, minimizing the battery's energy loss. The battery's energy loss consists of two parts: internal loss and external loss. The internal loss is the energy capacity fade at the end of discharge due to the low temperature. The external loss is the consumed energy that is not used for propelling the vehicle during driving. This energy includes the energy consumed by the heater and the thermal energy caused by the battery resistance. Hence, the cost function of this optimal control problem is established as follows:

$$\begin{aligned} J &= E_{loss\_in} + E_{loss\_ex} \\ &= E_{t0} - E_t\left(t_N\right) + \sum_{j=0}^{N-1}\left(I^2\left(R_o + R_p\right) + P_{heat}\right)\Delta t\left(k\right) \end{aligned} \tag{16}$$

where E_{loss_in} denotes the internal energy loss and E_{loss_ex} denotes the external energy loss. E_{t0} is the nominal energy capacity of the cell at normal temperature. Note that we assume that each cell in the battery pack is identical; thus, the cost function is for a single cell unit in the pack.

Dynamic programming (DP) is a widely used approach for solving discrete and multistage optimization problems and achieving global optimality. However, the DP algorithm also has drawbacks in real-world applications. For this particular problem, due to the backward solution mechanism of DP, the driving cycle must be predetermined, which makes it difficult to apply the algorithm for online cases. However, solving an offline optimal problem using the DP approach is a good choice for rule-based control design. Therefore, a constant- speed driving cycle was chosen here which can further reduce the computational load. Because the control problem is solved for a special case, the solution is not globally optimal and will be named by suboptimal control.

Based on the cost function defined in (16), the heating process is divided into N phases, with every decrease of 1% SOE in each phase and with $\Delta t(k)$ as the time interval of phase k. In other words, the initial condition of SOE should be $N\%$.

$$SOE\left(k+1\right) = SOE\left(k\right) - 0.01 \tag{17}$$

Combining (13) and (17), it is not difficult to obtain the time interval $\Delta t(k)$, as shown in (18), as shown at the bottom of the page.

The terminal time t_N is subject to the terminal condition that

$$SOE\left(t_N\right) = 0 \tag{19}$$

Because the nominal energy capacity of a cell is a constant, it is not necessary to include the E_{t0} term in the cost function. For the convenience of control design and implementation, the control effort remains unchanged within each phase. Furthermore, because the time interval is short, the current flowing through the cell could also be considered as a constant within each phase, as well as the resistances R_o and R_p. Then the cost function can be redefined as

$$\begin{aligned} J = -E_t\left(N\right) + \sum_{k=0}^{N-1}\Big(I^2\left(k\right)\left(R_o\left(k\right) + R_p\left(k\right)\right) \\ + P_{heat}\left(k\right)\Big)\Delta t\left(k\right) \end{aligned} \tag{20}$$

From (11) and (18), it can be seen that $T(k+1)$ is a function of $T(k)$ and $P_{heat}(k)$ with a fixed environmental temperature. By choosing T as the state variable and P_{heat} as the control input, the state equation can be written as

$$T\left(k+1\right) = \psi\left(T\left(k\right), P_{heat}\left(k\right)\right) \tag{21}$$

From (8), (9) and (18), the external energy loss in each phase is also a function of $T(k)$ and $P_{heat}(k)$, and we can define

$$\varphi\left(k\right) = \left(I^2\left(k\right)\left(R_o\left(k\right) + R_p\left(k\right)\right) + P_{heat}\left(k\right)\right)\Delta t\left(k\right) \tag{22}$$

Let $V*(k, T(k))$ be the optimal cost-to-go at step k for $k = N-1, N-2, \ldots, 0$, and it can be defined by the following equations:

$$\begin{cases} V^*\left(N, T\left(N\right)\right) = -E_t\left(T\left(N\right)\right) \\ V^*\left(k, T\left(k\right)\right) \\ \quad = \min\left[V^*\left(k+1, T\left(k+1\right)\right) + \varphi\left(k, T\left(k\right)\right)\right] \end{cases} \tag{23}$$

$$\Delta t\left(k\right) = \frac{0.01mC}{a\left(k\right)\left[I^2\left(k\right)\left(R_o\left(k\right) + R_p\left(k\right)\right) + \eta P_{heat}\left(k\right) - h_2A_2\left(T\left(k\right) - T_\infty\right)\right]E_c\left(k\right) - \left[P_{load}\left(k\right) + I^2\left(k\right)\left(R_o\left(k\right) + R_p\left(k\right)\right) + P_{heat}\left(k\right)\right]E_t\left(k\right)} \tag{18}$$

Then the optimal control $P_{opt}(k)$ can be solved by backward DP for $k = N-1, N-2, \ldots, 0$ as a function of $T(k)$ and subject to the constraint

$$P_{opt}(k) \in [P_{\min}, P_{\max}] \tag{24}$$

The resulting sequence of $P_{opt}(k)$ depends on the values of N (initial SOE) and $T(0)$, which implies that for different initial SOE and temperature conditions, the optimal heating power could vary. However, based on the principle of optimality, the solution of P_{opt} at each point of the SOE and temperature is unique despite the different initial conditions. In other words, the instantaneous value of P_{opt} only depends on the battery SOE and temperature at the current stage, which makes it convenient to control implementation in real-time applications. Instead of being solved online, the optimal control P_{opt} is computed offline for different cases, and the values are stored in a lookup table. Note that the environmental temperature also affects the results; thus, the optimal control will be computed for several different T_∞ cases and the final control P_{opt} is obtained by linear interpolation between lookup tables. Figure 6 shows the result at -20°C environmental temperature.

IV. RESULTS AND DISCUSSIONS

A. TEST SETUP

The experimental platform is illustrated in Figure 7. A Neware 8008 battery testing system was used to charge/discharge the battery cells. The testing system has a maximum 25V and 500A operating range and can perform tests at the cell and module levels. The data acquisition function is integrated into the testing system, and the voltage and temperature information of the cells were captured and recorded on a host computer. The tested cells were placed in the temperature chamber, which has a temperature operating range of -40°C to $+150$°C. In open loop tests, a DC power supply was used to drive the external heater at constant power levels to identify the thermal parameters.

B. MODEL VALIDATION

First, several short-distance real-world driving data with the target vehicle were taken to validate the equivalent circuit model. The data covered a wide SOE and temperature operating range, and two cases were chosen to show the results. The data with respect to Figure 8 were taken with an initial condition of 92% SOE and -23°C with a smaller current (due to the limited capability of the battery), while in Figure 9 it was taken with an initial condition of 64% SOE and -6°C with a larger current. It can be seen that for both cases the simulated voltage by the equivalent circuit model matches the experimental data very well, which implies that the parameters of the battery were well calibrated, and this model was sufficient to predict the internal heating behavior of the battery.

Second, long-distance real-world driving data were used to validate the thermal model. The target vehicle was soaked overnight at -29°C environmental temperature. The driving

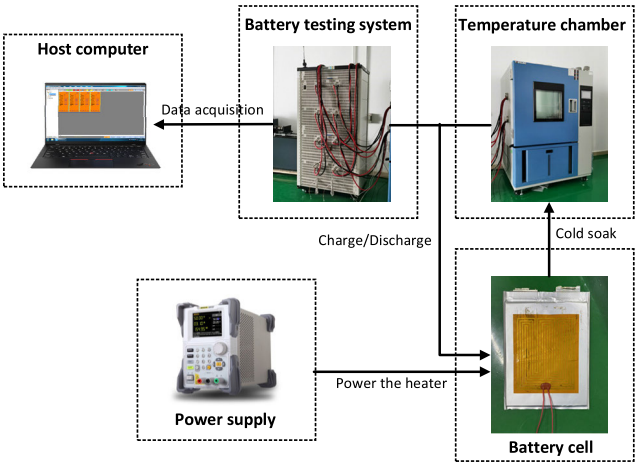

FIGURE 7. Test setup.

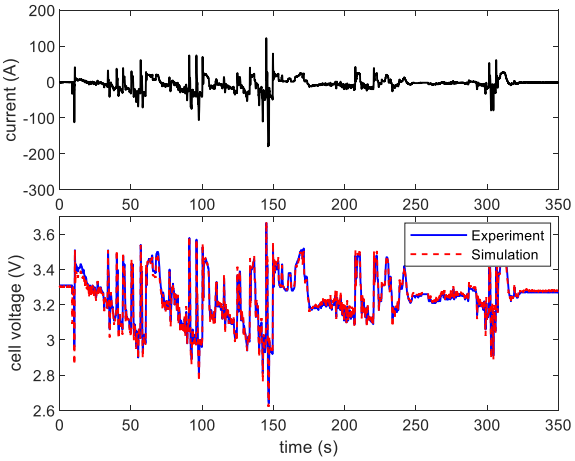

FIGURE 8. Equivalent circuit model validation at -23°C.

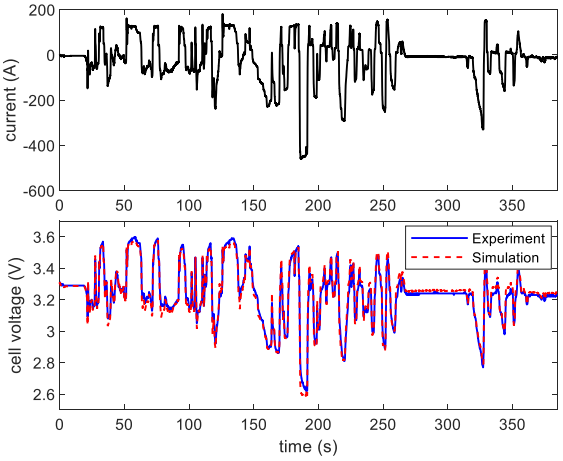

FIGURE 9. Equivalent circuit model validation at -6°C.

cycle started with a battery initial condition of -24°C average cell temperature and 70% SOE. The ambient temperature was -4°C. The driving cycle took 2880 s with mixed driving styles, such as mild acceleration and deceleration, aggressive

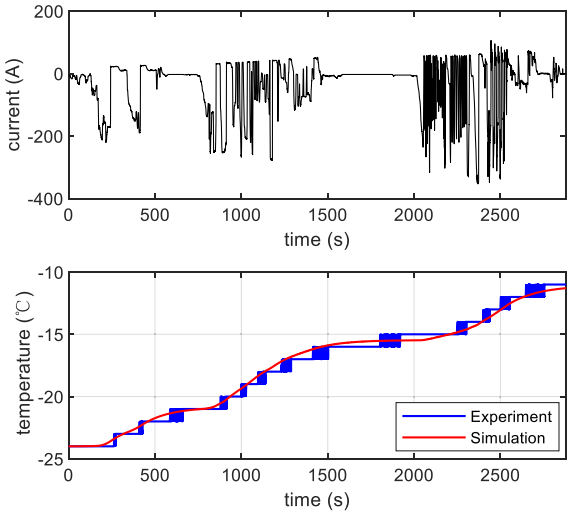

FIGURE 10. Thermal model validation for long distance driving.

acceleration and braking, and long-time coasting. The average cell temperature was captured using a temperature sensor with resolution of 1°C. Figure 10 compares the simulated cell temperature to the experimental data and shows that the proposed battery model can provide an accurate prediction within a large operating range.

Third, an external heating test was performed to validate the thermal model. A module equipped with the proposed electrothermal films was soaked in the temperature chamber and the temperature was stabilized at −20°C. The heater was then operated at a constant power of 15 W for each film. The heating procedure lasted for 2 h, followed by a constant temperature soak for 2 h. Both the cell temperature and film temperature were recorded by temperature sensors embedded in the battery testing system. From Figure 11 it can be seen that the temperature estimation error is less than ±0.5°C for most of the time, and the maximum error occurs at the beginning of the heating mainly because of the dynamic response of the sensor and the heat transfer inside the cell.

Based on the experimental validation listed above, it was confirmed that the developed model has satisfactory fidelity to simulate the electrical and thermal behavior of the battery, and it could be used in the simulation to validate the rule-based external heating strategy as explained in the following section.

C. SIMULATION RESULT

The proposed rule-based control strategy was then evaluated by simulation. A complete vehicle dynamic model was run to obtain the total required power of the target battery pack, along with the developed battery electrical and thermal model to provide the SOE and temperature information. EPA driving cycles were adopted to evaluate the benefits of the rule-based control.

The first case was the HWFET driving cycle, and several repeated HWFET cycles were connected because the range of an EV with a fully charged battery is much longer than that

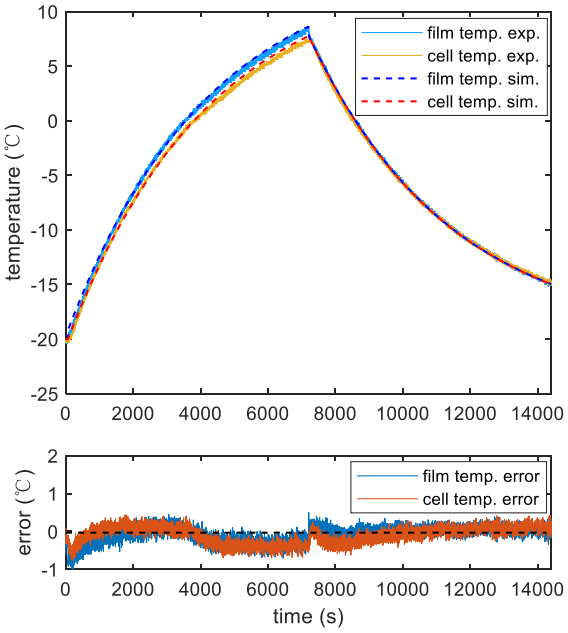

FIGURE 11. Constant power external heating at −20°C.

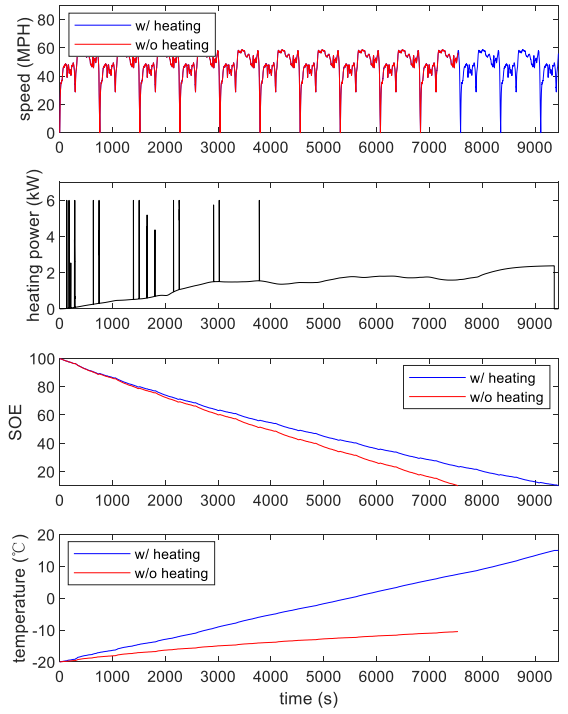

FIGURE 12. Repeated HWFET driving cycle simulation.

of a single driving cycle. The initial battery SOE was 100%, and both the initial cell temperature and environmental temperature were −20°C. Simulation results show that by applying the rule-based heating control, the total range reached 126.3 miles, while it was 101.2 miles without heating, and 24.7% improvement was achieved.

From Figure 12, it can be seen that without heating, the cell temperature rose to −10.5°C due to the internal resistance of

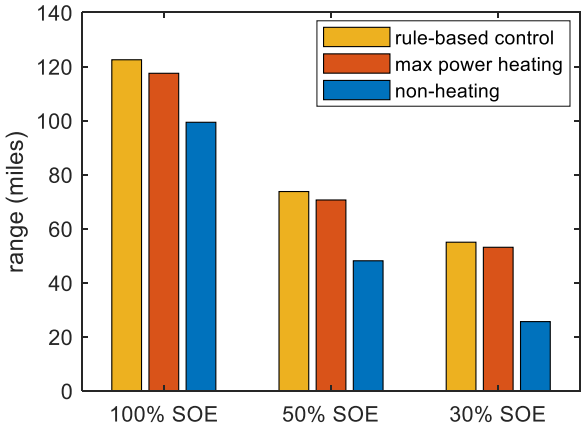

FIGURE 13. UDDS driving cycle comparison with different initial SOE.

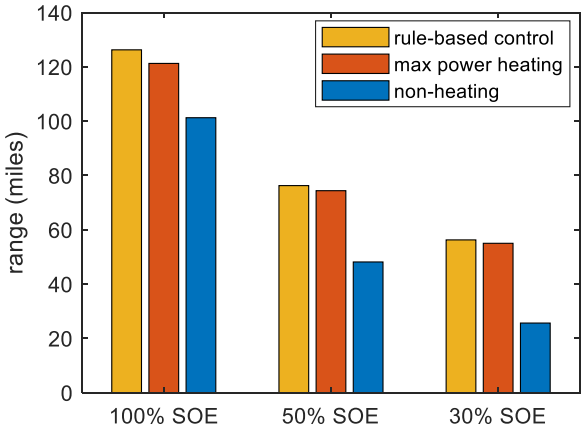

FIGURE 14. HWFET driving cycle comparison with different initial SOE.

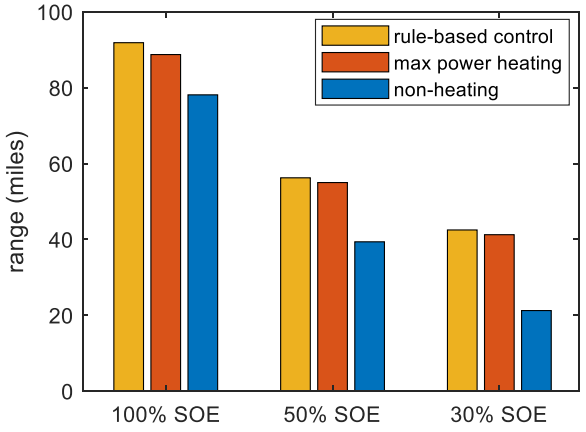

FIGURE 15. US06 driving cycle comparison with different initial SOE.

the battery; while with heating, the final temperature reached +15.2°C and the battery recovered its full capacity. The heating power is shown in the second subplot of Figure 12, and several ''spikes'' before 4000 s denote the full use of heating power when the battery was not capable of absorbing all the regenerative power.

Second, different driving cycles with different initial conditions were investigated. Figure 13 shows the comparison between the three strategies for the UDDS driving cycle: rule-based control, maximum (constant) power heating control and without external heating. The maximum power heating control is the strategy in which the heating power remains constant at 6 kW, which is the maximum power of the heater of the entire pack, until the cell temperature reaches the target.

Three cases with different initial SOEs were studied. When the initial SOE of the battery was 100%, the total ranges under the three strategies were 122, 118 and 99 miles, respectively. Compared with the maximum power heating and non-heating strategies, the proposed rule-based control achieved 4.3% and 23.2% improvement in the total range, respectively. When the initial SOE was 50%, the corresponding improvements were 4.4% and 53.2%. When the initial SOE was 30%, the corresponding improvements were 2.3% and 114.6%. Obviously, a larger improvement can be obtained with a lower initial SOE. The main reason is that starting with a lower initial SOE without external heating causes the battery to run out of available energy before it can be heated by internal resistance heating. Starting with a higher initial SOE gives the battery a longer time for internal heating, so it obtains a better capacity recovery before the SOE drops to the end.

In addition, rule-based control also shows improvement compared with maximum power heating control for two main reasons: 1) maximum power heating requires more power from the battery, which results in larger internal heat loss; 2) maximum power heating increases the temperature faster, which results in more heat transfer to the cold environment.

Figure 14 shows a comparison for the HWFET driving cycles. Similar results were observed: starting with 100% SOE, the corresponding improvement was 4.1% and 24.7%. Starting with 50% SOE, the corresponding improvement was 2.5% and 58.4%; starting with 30% SOE, the corresponding improvement was 1.1% and 119.5%.

In contrast to the UDDS driving cycle results, the improvement between rule-based control and maximum power control is not significant, especially at lower initial SOEs. This is mainly due to the faster average vehicle speed of the HWFET cycle, which requires a larger heating power to heat the battery before the SOE drops to the end. The resulting optimal power obtained from rule-based control is quite close to the maximum power.

Figure 15 shows the same comparison for the US06 driving cycle. The overall achieved range is much shorter than the previous two driving cycles because of the high-speed and aggressive driving style of the US06 cycle, which consumes more energy per unit distance. Two phenomena can also be observed. One is that the improvement between rule-based control and non-heating control with higher initial SOE is not as significant as that achieved in the other two driving cycles (17.6% with 100% initial SOE). The lower capacity loss of the non-heating battery system is attributed to the stronger internal heating effect caused by the large power request of the US06 driving cycle. The other is that for low initial

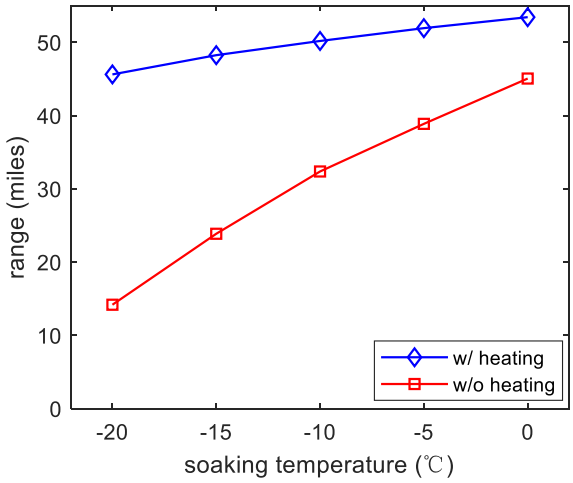

FIGURE 16. UDDS driving cycle comparison with different soaking temperature.

SOE cases, the range has been greatly reduced again due to the low final temperature. Furthermore, the highly limited battery discharging capability cannot satisfy the requirement of aggressive acceleration; thus the speed profile could not be followed very well.

Finally, an overnight cold soak case was studied. It was assumed that the car finished a day of driving with an ending SOE of 50% and warm battery temperature and was cold soaked in the garage without charging for a whole night at different temperatures. The next day the car drove in a medium cold environment at 0°C. Five cases with different soaking temperatures were simulated, from −20°C to 0°C. Figure 16 shows the results of a comparison between external heating and non-heating. The largest difference occurred at the lowest soaking temperature; at −20°C the vehicle only got 14.2 miles range without external heating, while with external heating, the total range increased to 45.6 miles and 220% improvement was achieved. Even at 0°C, external heating can help gain 18.6% more range, and the total range with external heating also increased to 53.4 miles. Note that in warm temperatures the normal range with 50% initial SOE is 61.8 miles, which means that in extremely cold weather such as −20°C, the range loss under the external heating control is only one-third of that without the external heating.

V. CONCLUSION

A battery external heating system using electrothermal film and a rule-based heating control strategy for electric vehicle driving at low temperatures were developed in this study, based on an equivalent circuit model and thermal model, which were proven to have high fidelity through experimental and real-world driving tests. Dynamic programming algorithm was applied to maximize the total driving range of the vehicle for a special case, and the suboptimal solution was combined with other rules to deal with wide operating conditions. Simulation results show that the proposed algorithm can significantly improve the ''shortened range'' problem in cold weather. Compared with the vehicle without external heating, the proposed approach increased the total range by 18.6% to 220% for different driving conditions. These improvements were gained by warming up the battery during driving to recover the available energy capacity. Compared with the maximum power heating control method, the proposed approach showed an improvement of 1.1% to 4.4% by optimizing the trade-off between temperature rise and energy consumption/loss. In addition, owing to its small size and low computational load, the developed external heating system is suitable for onboard implementation.

REFERENCES

[1] Y. A. Wu, A. W. Ng, Z. Yu, J. Huang, K. Meng, and Z. Y. Dong, ''A review of evolutionary policy incentives for sustainable development of electric vehicles in China: Strategic implications,'' *Energy Policy*, vol. 148, Jan. 2021, Art. no. 111983.

[2] C. Capasso and O. Veneri, ''Experimental analysis on the performance of lithium based batteries for road full electric and hybrid vehicles,'' *Appl. Energy*, vol. 136, pp. 921–930, Dec. 2014.

[3] J. Jaguemont, L. Boulon, and Y. Dubé, ''A comprehensive review of lithium-ion batteries used in hybrid and electric vehicles at cold temperatures,'' *Appl. Energy*, vol. 164, pp. 99–114, Feb. 2016.

[4] M. C. Smart, B. V. Ratnakumar, A. Behar, L. D. Whitcanack, J.-S. Yu, and M. Alamgir, ''Gel polymer electrolyte lithium-ion cells with improved low temperature performance,'' *J. Power Sources*, vol. 165, no. 2, pp. 535–543, Mar. 2007.

[5] S. S. Zhang, K. Xu, and T. R. Jow, ''The low temperature performance of Li-ion batteries,'' *J. Power Sources*, vol. 115, no. 1, pp. 137–140, 2003.

[6] X. Gong and C. C. Mi, ''Temperature-dependent performance of lithium ion batteries in electric vehicles,'' in *Proc. IEEE Appl. Power Electron. Conf. Expo. (APEC)*, Mar. 2015, pp. 1065–1072.

[7] J. R. M. Delos Reyes, R. V. Parsons, and R. Hoemsen, ''Winter happens: The effect of ambient temperature on the travel range of electric vehicles,'' *IEEE Trans. Veh. Technol.*, vol. 65, no. 6, pp. 4016–4022, Jun. 2016.

[8] T. A. Stuart and A. Hande, ''HEV battery heating using ac currents,'' *J. Power Sources*, vol. 129, no. 2, pp. 368–378, 2004.

[9] K. Liu, K. Li, Q. Peng, and C. Zhang, ''A brief review on key technologies in the battery management system of electric vehicles,'' *Frontiers Mech. Eng.*, vol. 14, no. 1, pp. 47–64, Mar. 2019.

[10] S. Wu, R. Xiong, H. Li, V. Nian, and S. Ma, ''The state of the art on preheating lithium-ion batteries in cold weather,'' *J. Energy Storage*, vol. 27, Feb. 2020, Art. no. 101059.

[11] Y. Ji and C. Y. Wang, ''Heating strategies for Li-ion batteries operated from subzero temperatures,'' *Electrochim. Acta*, vol. 107, pp. 664–674, Sep. 2013.

[12] Z. Song, H. Hofmann, J. Li, J. Hou, X. Zhang, and M. Ouyang, ''The optimization of a hybrid energy storage system at subzero temperatures: Energy management strategy design and battery heating requirement analysis,'' *Appl. Energy*, vol. 159, pp. 576–588, Dec. 2015.

[13] J. Zhang, F. Sun, and Z. Wang, ''Heating character of a $LiMn_2O_4$ battery pack at low temperature based on PTC and metallic resistance material,'' *Energy Proc.*, vol. 105, pp. 2131–2138, May 2017.

[14] Z. Lei, C. Zhang, J. Li, G. Fan, and Z. Lin, ''Preheating method of lithium-ion batteries in an electric vehicle,'' *J. Modern Power Syst. Clean Energy*, vol. 3, no. 2, pp. 289–296, Jun. 2015.

[15] C. Alaoui and Z. M. Salameh, ''A novel thermal management for electric and hybrid vehicles,'' *IEEE Trans. Veh. Technol.*, vol. 54, no. 2, pp. 468–476, Mar. 2005.

[16] M. Chen and J. Li, ''Experimental study on heating performance of pure electric vehicle power battery under low temperature environment,'' *Int. J. Heat Mass Transf.*, vol. 172, Jun. 2021, Art. no. 121191.

[17] H. Ruan, J. Jiang, B. Sun, W. Zhang, W. Gao, L. Y. Wang, and Z. Ma, ''A rapid low-temperature internal heating strategy with optimal frequency based on constant polarization voltage for lithium-ion batteries,'' *Appl. Energy*, vol. 177, pp. 771–782, Sep. 2016.

[18] L. Zhang, W. Fan, Z. Wang, W. Li, and D. U. Sauer, "Battery heating for lithium-ion batteries based on multi-stage alternative currents," *J. Energy Storage*, vol. 32, Dec. 2020, Art. no. 101885.
[19] Y. Shang, K. Liu, N. Cui, Q. Zhang, and C. Zhang, "A sine-wave heating circuit for automotive battery self-heating at subzero temperatures," *IEEE Trans. Ind. Informat.*, vol. 16, no. 5, pp. 3355–3365, May 2020.
[20] Y. Li, J. Du, G. Zhou, M. Ouyang, and Y. Fan, "A rapid self-heating battery pack achieved by novel driving circuits of electric vehicle," *Energy Rep.*, vol. 6, pp. 1016–1023, Dec. 2020.
[21] Y. Shang, C. Zhu, G. Lu, Q. Zhang, N. Cui, and C. Zhang, "Modeling and analysis of high-frequency alternating-current heating for lithium-ion batteries under low-temperature operations," *J. Power Sources*, vol. 450, Feb. 2020, Art. no. 227435.
[22] G. Ning, B. Haran, and B. N. Popov, "Capacity fade study of lithium-ion batteries cycled at high discharge rates," *J. Power Sources*, vol. 117, nos. 1–2, pp. 160–169, 2003.
[23] J. Du, Z. Chen, and F. Li, "Multi-objective optimization discharge method for heating lithium-ion battery at low temperatures," *IEEE Access*, vol. 6, pp. 44036–44049, 2018.
[24] H. Ruan, J. Jiang, B. Sun, X. Su, X. He, and K. Zhao, "An optimal internal-heating strategy for lithium-ion batteries at low temperature considering both heating time and lifetime reduction," *Appl. Energy*, vol. 256, Dec. 2019, Art. no. 113797.
[25] Y. Qin, J. Du, L. Lu, M. Gao, F. Haase, J. Li, and M. Ouyang, "A rapid lithium-ion battery heating method based on bidirectional pulsed current: Heating effect and impact on battery life," *Appl. Energy*, vol. 280, Dec. 2020, Art. no. 115957.
[26] C. Y. Wang, G. Zhang, S. Ge, T. Xu, Y. Ji, X. G. Yang, and Y. Leng, "Lithium-ion battery structure that self-heats at low temperatures," *Nature*, vol. 529, no. 7587, p. 515, 2016.

SHUPENG ZHANG (Member, IEEE) received the B.S. and M.S. degrees in automotive engineering from Tsinghua University, Beijing, China, in 2006 and 2009, respectively, and the Ph.D. degree in mechanical engineering from Michigan State University, MI, USA, in 2014.

He is currently an Associate Professor with the College of Urban Transportation and Logistics, Shenzhen Technology University, Guangdong, China. Prior to joining the university, he was a Control System Engineer of vehicle control with Karma Automotive LLC, CA, USA. His current research interests include modeling and control of internal combustion engines, hybrid vehicle powertrain control and optimization, and advanced control theory and applications.

WENJING SHEN (Member, IEEE) received the B.E. and M.E. degrees in mechatronics engineering from Central South University, Changsha, China, in 2006 and 2009, respectively, and the Ph.D. degree in systems engineering and engineering management from the City University of Hong Kong, in 2017.

She is currently an Associate Professor with the Sino-German College of Intelligent Manufacturing, Shenzhen Technology University, Guangdong, China. Her current research interests include modeling of thermal distribution in industrial processes, data-based modeling, and optimization.